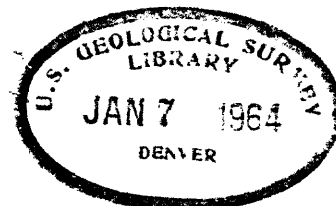


POLAR CHARTS FOR CALCULATING AEROMAGNETIC
ANOMALIES OF THREE-DIMENSIONAL BODIES

by

R. G. Henderson and Alphonso Wilson
U. S. Geological Survey
Washington, D. C.



Introduction

When it is possible to make reasonable assumptions about the depth, size, shape, and magnetization of a three-dimensional body which cannot sensibly be represented by a simple geometric form, recourse must be made to approximation calculations.

The method presented here enables one to calculate the aeromagnetic anomaly of three-dimensional bodies of arbitrary shape with the aid of graticules constructed for each of seven inclinations of the earth's magnetic field. This method continues to find use when only a few computed points are desired, even though elaborate computer programs and machinery may be available.

U. S. Geological Survey
OPEN FILE REPORT 64-76

This report is preliminary and has not been edited or reviewed for conformity with Geological Survey standards or nomenclature.

~~Publication authorized by the Director, U. S. Geological Survey.~~

A preliminary account of the method was given by Henderson (1960). A more complete account is given in the S.E.G. Mining Volume (Henderson and Wilson, 1963) where plates 1-7 are presented at small scale for photographic reproduction. The purpose of this release is to provide access to large scale negatives of the plates from which positive prints can be made on transparent media at 1:1 or larger scale. The method is explained here as it applies to three fundamental cases; it is also shown how the chart for inclination $I = 90^\circ$ can be used in gravity calculations.

The charts

In aeromagnetic work the component of the total magnetic intensity anomaly in the direction of the earth's total field vector is represented by ΔT . The graticules are based on the formula for the ΔT anomaly at a point (see figure 1) caused by an elemental semi-infinite vertical cylindrical sector at unit depth below the plane of observations and magnetized by induction in the earth's field. The point P at which the effect is to be determined is taken as the origin of a right hand coordinate system with x positive towards magnetic north and z positive downward. All lengths are presumed to have been divided by the depth so that in the discussion which follows the radius r is a dimensionless ratio. The ΔT anomaly per unit magnetization at P due to the element is

$$\begin{aligned}
\left(\frac{\Delta T}{k T_0} \right)_{\text{element}} &= (\sin \theta_{j+1}, \cos \theta_{j+1}, -\sin \theta_j, \cos \theta_j) \left\{ \cos^2 I \left[\ln \frac{1 + \sqrt{r_{j+1}^2 + 1}}{1 + \sqrt{r_j^2 + 1}} + \frac{1}{2} \left(\frac{1}{\sqrt{r_{j+1}^2 + 1}} - \frac{1}{\sqrt{r_j^2 + 1}} \right) \right] \right\} \\
&+ (\sin \theta_{j+1} - \sin \theta_j) \left\{ 2 \sin I \cos I \left[\ln \frac{r_{j+1} + \sqrt{r_{j+1}^2 + 1}}{r_j + \sqrt{r_j^2 + 1}} - \left(\frac{r_{j+1}}{\sqrt{r_{j+1}^2 + 1}} - \frac{r_j}{\sqrt{r_j^2 + 1}} \right) \right] \right\} \\
&+ (\theta_{j+1} - \theta_j) \left\{ \left(\sin^2 I - \frac{1}{2} \cos^2 I \right) \left[\frac{1}{\sqrt{r_{j+1}^2 + 1}} - \frac{1}{\sqrt{r_j^2 + 1}} \right] \right\} \quad (1)
\end{aligned}$$

In (1) k is the magnetic susceptibility of the element and T_0 is the magnitude of the earth's normal field. Using (1) and requiring that each element on a chart have the same prescribed value $(\Delta T/k T_0) = \alpha$, called the chart constant, we constructed graticules for use at magnetic inclinations $I = 0^\circ, 20^\circ, 30^\circ, 45^\circ, 60^\circ, 75^\circ$, and 90° . For a given inclination an α was chosen which would make the chart convenient to use, but where possible it was made a preassigned decimal fraction of the half-space anomaly, $(\Delta T/k T_0) = \pi (2 \sin^2 I - \cos^2 I)$. The constants and plate numbers for the various inclinations are given in Table 1.

Table 1

Plate Number	1	2	3	4	5	6	7
Inclination	0°	20°	30°	45°	60°	75°	90°
α in gammas per unit magnetization	0.00314	0.00306	0.00312	0.00312	0.00393	0.00565	0.00314

A typical polar chart, for $I = 45^\circ$, is shown in Figure 2. Each complete element contributes at the center a total magnetic intensity effect of 0.00312 gamma: per unit magnetization. The elemental value was not always contained in the extrema ranges of θ an integral number of times, hence some elements have less than full value. A number inserted in a fractional element indicates the percent of a full value it receives. For example, the number 38 appearing in an element means that it receives 0.38 of a chart value.

Account must be taken of the algebraic sign of elements. In general, positive and negative areas are set off by broken lines, and are indicated by + and - signs. For $I = 0^\circ$ and $I = 20^\circ$ there is a central area enclosed in a heavy circle in which all the elements are negative. Outside this circle there are positive areas north and south and negative areas east and west. From $I = 30^\circ$ to $I = 75^\circ$ there is one positive area north and one negative area south on each chart. The positive area increases from chart to chart with the inclination until at $I = 90^\circ$, the elements are all positive.

Because the ruled radial lines become dense in the neighborhood of the center and tend to obscure its exact location a small area about the center has been arbitrarily deleted from each chart.

The charts can be reproduced on a transparent medium at any convenient scale; however, for this report we have chosen a standard scale of 1/2 inch equals a depth unit.

Use of charts

The application to a basic semi-infinite body will be explained in detail. The extension to other bodies is but a corollary.

Semi-infinite vertical cylinder

Consider a vertical cylinder whose upper base, enclosed by a regular contour C_0 as shown in Figure 3, is at depth z_0 , and whose lower base, for the moment, is infinitely remote, i.e., the depth extent is infinite. Suppose that the inducing field has an inclination $I = 60^\circ$ and a magnitude T_0 ; that the susceptibility of the cylinder exceeds that of the surrounding material by an amount k , and that the anomaly is to be computed at points P_1 , P_2 , and P_3 . We use the graticule at $I = 60^\circ$. The contour C_0 together with the points P_1 , P_2 , P_3 is plotted at a scale $z_0 = 1/2$ inch. A straight line in the direction of magnetic north is drawn through each of the points. The chart is centered at a point to be computed, say P_1 , with its magnetic axis pointing towards magnetic north. The elements covering the area within the contour are counted with regard to sign, i.e., a positive element receives a positive count, a negative element receives a negative count. The interior portions of elements cut by the contour C_0 are given a proportionate fractional count. The positive and negative counts are added algebraically. Suppose the summed count is $N(z_0)$. Then the anomaly at P_1 in gammas per unit magnetization is $4N(z_0)$. For $I = 60^\circ$ (see Table 1), $\alpha = 0.00393$.

The anomaly in gammas is then

$$\Delta T = k T_0 (0.00393) N(z_0)$$

The chart would be similarly centered and aligned and the covering elements counted at any subsequent points such as P_2 and P_3 .

Finite cylindrical bodies; laminae

Suppose the cylinder in Figure 3 has a finite depth extent, t , with lower base at $z_1 = z_0 + t$ as shown also in Figure 3. To compute its anomaly at P_1 , we calculate the anomaly of a second semi-infinite cylinder, this time with the depth to the "upper" base equal to z_1 and subtract the effects of the second from the first. The same chart can be used on the second cylinder if we adjust the scale of its configuration so that $z_1 = 1/2$ inch. The configuration consisting of the contour together with all the points to be computed is so reduced to scale. The configuration reduced about P_2 is shown in Figure 3 with points to be computed now shown in primed notation. The chart is now used at P'_1 , P'_2 , and P'_3 in turn. Let $N(z_1)$ be the number of counts for the lower semi-infinite cylinder at P'_1 , then the anomaly due to the finite cylinder will be

$$\Delta T = k T_0 (0.00393) [N(z_0) - N(z_1)],$$

$N(z_0)$ being the number of counts determined for the same point for the upper cylinder.

When the depth extent, t , is much less than the depth of burial z_0 , we have the case of a lamina. Laminas and the superposition principle are the bases for the general three-dimensional case discussed below.

Three-dimensional body of arbitrary shape

A three-dimensional body may be approximated by a set of flat lying laminas and represented by a contour map. The laminas need not have the same thickness; in fact it is consistent with the attenuation properties of anomalies to take the layers thicker for increasing z . This results in more rapid computations.

The layered body is initially contoured with z_0 as chart depth as shown in Figure 4a. Configuration reductions to scale are made at each depth z_1 and the computations for each layer are performed as explained above. If $N(z_{i-1}, p)$ is the number of counts at P due to the i -th layer, then the effect due to the entire body is

$$\Delta T = k T_0 \alpha \sum_{i=1}^n N(z_{i-1}, p) \quad \text{where} \quad N(z_{i-1}, p) = N(z_{i-1}) - N(z_i)$$

and α is the chart constant.

In cases where the three-dimensional body has considerable depth extent and would involve too many laminas, it is preferable to conceive the body as composed of a nest of vertical (not necessarily circular) cylinders. The chart is then used at the top and bottom of a central cylinder and at the tops and bottoms of several surrounding cylindrical shells. In this way the computations may be effected more rapidly.

Gravity calculations

At inclination $I = 90^\circ$, equation (1) for a magnetic element reduces to

$$\left(\frac{\Delta T}{k T_0} \right)_{\text{mag element}} = (\theta_{j+1} - \theta_j) \left(\frac{1}{\sqrt{r_{j+1}^2 + 1}} - \frac{1}{\sqrt{r_j^2 + 1}} \right) \quad (2)$$

The right member of (2) is a numeric which can be shown to be proportional to Δg , the vertical component of gravity at P due to an element dz units thick. More precisely, for a mass element

$$\left(\frac{\Delta g}{G \rho dz} \right)_{\text{mass element}} = (\theta_{j+1} - \theta_j) \left(\frac{1}{\sqrt{r_{j+1}^2 + 1}} - \frac{1}{\sqrt{r_j^2 + 1}} \right) \dots (3)$$

where G is the gravitational constant, and ρ is the density of the element. In view of the equivalence of (2) and (3), the chart at $I = 90^\circ$, with some change in concept, may be used in three-dimensional gravity calculations. In fact, it becomes simply a solid angle chart not unlike one designed by Lachenbruch (1957) for certain heat conduction problems. The accuracy of the $I = 90^\circ$ graticule as a solid angle chart can be readily established by applying it to a circular disc and comparing the resulting values with those given by Masket and Rodgers (1962).

The gravity application is well known and needs little or no elaboration. The body is divided into horizontal laminæ, but the chart is used at the median plane (Figure 4c) rather than at the top and bottom of a lamina, and the depths z_1 are to this plane.

The chart element is 2.089×10^{-5} milligals per meter per unit density. The gravity anomaly for a lamina is then

$$\Delta g = 2.089 \times 10^{-5} \rho N(z_1) dz_1$$

where $N(z_1)$ is the number of elements counted at the median plane.

In a mathematically rigorous sense, the lamina should have infinitesimal thickness, but practically, it need not be so. Nettleton (1942) discusses the error due to finite thickness in certain special cases.

For an approximation to the gravity effect at P due to the entire body, one could add up the effects of the various laminae, i.e.,

$$\Delta g = 2.089 \times 10^{-5} \sum N(z_1) \rho_i dz_1$$

The density ρ_i has been placed after the summation sign to allow for layerwise changes in density.

For more accurate values of the gravity effect one can follow Talwani and Ewing (1960) and perform a numerical integration after determining $N(z_1)$ at the various levels. It should be observed that our expression $2.089 \times 10^{-5} \rho N(z)$ corresponds to the V of Talwani and Ewing (1960). Their three-level system of integration can therefore be used once the values $2.089 \times 10^{-5} \rho N(z)$ have been determined.

Practical application

The following illustration of an application to a semi-infinite cylinder of irregular horizontal section is due to John W. Allingham of the U. S. Geological Survey. Figure 5 is an aeromagnetic map of the Pea Ridge anomaly in Washington County, southeast Missouri. The crystalline basement rocks are overlain by about 1,100 feet of Paleozoic sedimentary rocks. The buried contact between the rhyolitic volcanic rocks and the granite host rock, shown in heavy outline, was inferred from the magnetic map by the method given by Vacquier et al. (1951). The magnetic susceptibility of the granite was determined from drill hole samples and from outcrops in the neighboring St. Francois Mountains. Susceptibilities for the volcanic rocks were based on subsurface measurements in the Indian Creek area and in the area of Pilot Knob. Drilling has established the existence of a magnetite ore body. The shape of the body shown in the rectangle is essentially conjectural. The chart for $I = 75^\circ$ at a scale one inch equals one depth unit was used to compute profile A-A' as discussed above for a vertical cylinder, except that the body here is composite. The separate profiles computed for the volcanic rocks and the magnetite body in Figure 6, when combined, give an anomaly which closely fits the observed profile. In view of the ambiguity of such interpretations, this can only be regarded as one of many possible solutions.

For practical examples of "layer cake" type of approximations to three-dimensional bodies, the reader is referred to Henderson (1960) or Allingham and Zietz (1962).

Acknowledgments

The authors are grateful to John W. Allingham of the U. S. Geological Survey, whose persistent requests provided the early stimulus for this work, and whose practical applications were generously made available to them. Thanks are due to Emil Seginak who assisted in the drafting and to H. R. Joesting, Andrew Griscom, and other coworkers in the Survey who used the charts extensively and contributed valuable suggestions leading to their improvement.

References

- Allingham, J. W., and Zietz, Isidore, 1962, Geophysical data on the Climax Stock, Nevada Test Site, Nye County, Nevada: *Geophysics*, v. 27, no. 5, p. 599-610.
- Cassmann, Fritz, 1951, Graphical evaluation of the anomalies of gravity and of the magnetic field caused by three-dimensional bodies: World Petroleum Congress, 3d, The Hague, Proc., sec. 1, p. 613-621.
- Henderson, R. G., 1960, Polar charts for evaluating magnetic anomalies of three-dimensional bodies: Article 52, in U. S. Geological Survey Prof. Paper 400-B, p. B112-B114.
- Henderson, R. G., and Wilson, Alphonso, 1963, Polar charts for calculating aeromagnetic anomalies of three-dimensional bodies: S.E.G. Mining Volume (in press).
- Lachenbruch, A. H., 1957, Three-dimensional heat conduction in permafrost beneath heated buildings: U. S. Geol. Survey Bull. 1052-B, p. 50-69.
- Masket, A. V. H., and Rodgers, W. C., 1962, Tables of Solid Angles; U. S. Atomic Energy Commission Rept., TID-14975.
- Nettleton, L. L., 1942, Gravity and magnetic calculations: *Geophysics*, v. 7, no. 3, p. 293-310.
- Talwani, Manik, and Ewing, Maurice, 1960, Rapid computation of gravitational attraction of three-dimensional bodies of arbitrary shape: *Geophysics*, v. 25, no. 1, p. 203-225.

Vacquier, Victor, Steenland, N. C., Henderson, R. G., and Zietz,
Isidore, 1951, Interpretation of aeromagnetic maps: Geol. Soc.
America Mem. 47.

54544

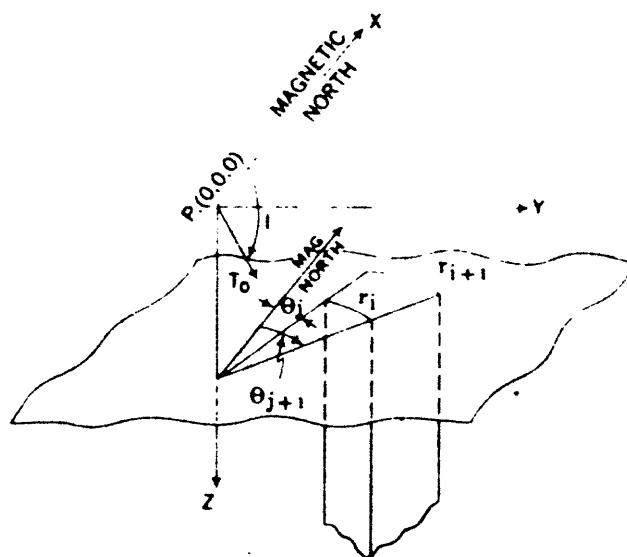
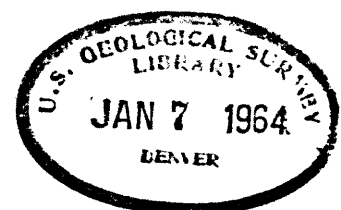


Figure 1. Elemental semi-infinite vertical cylindrical sector in relation to coordinate system. The effect at P is the basis of the charts.

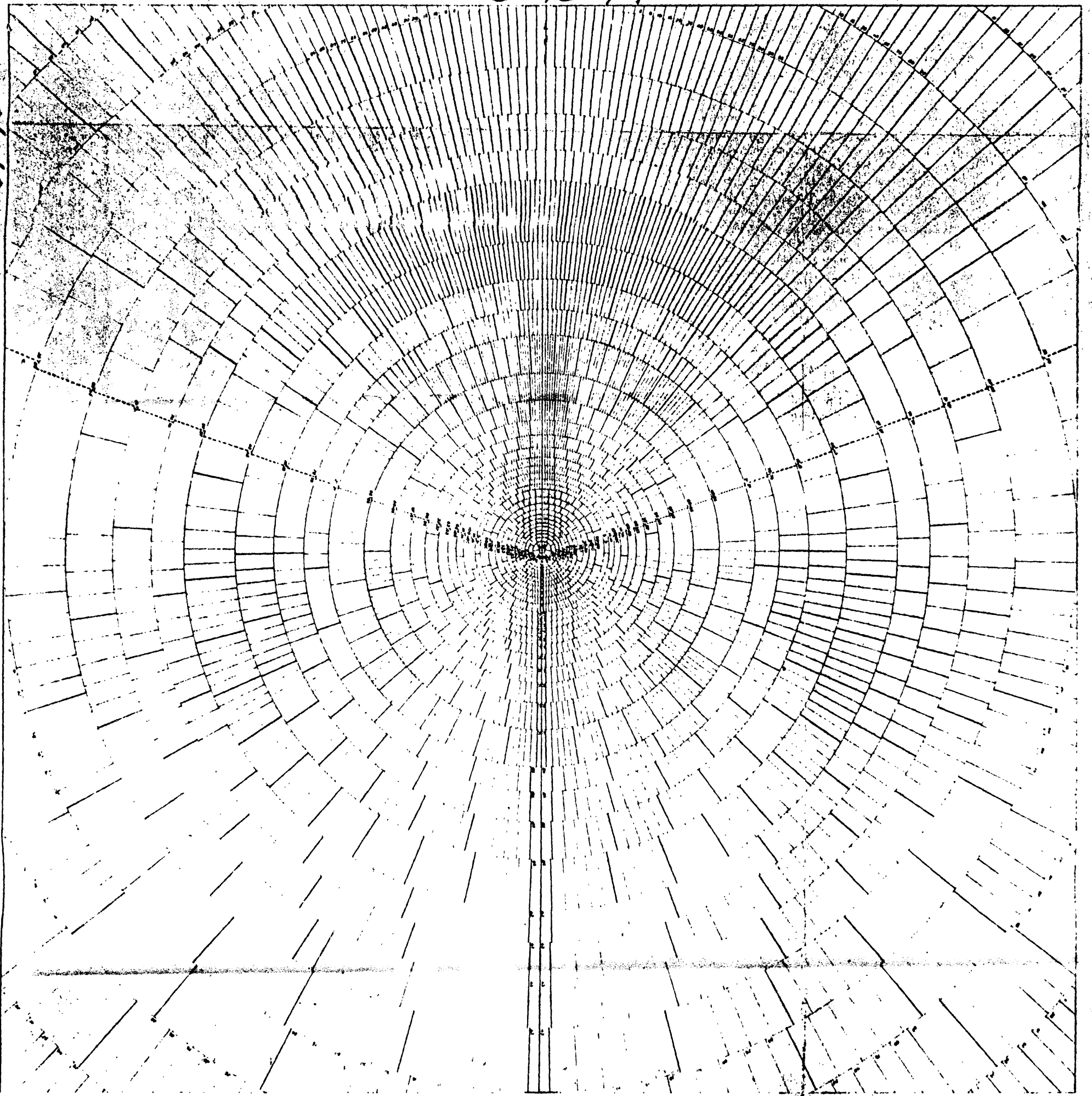
PLEASE REPLACE IN POCKET
IN BACK OF BOUND VOLUME

54544



54544

64-76



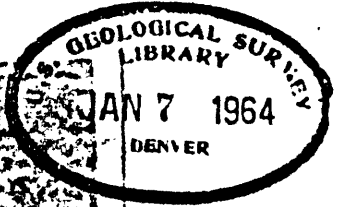
INCLINATION $I = 45^\circ$ SECTOR VALUE = 0.00312

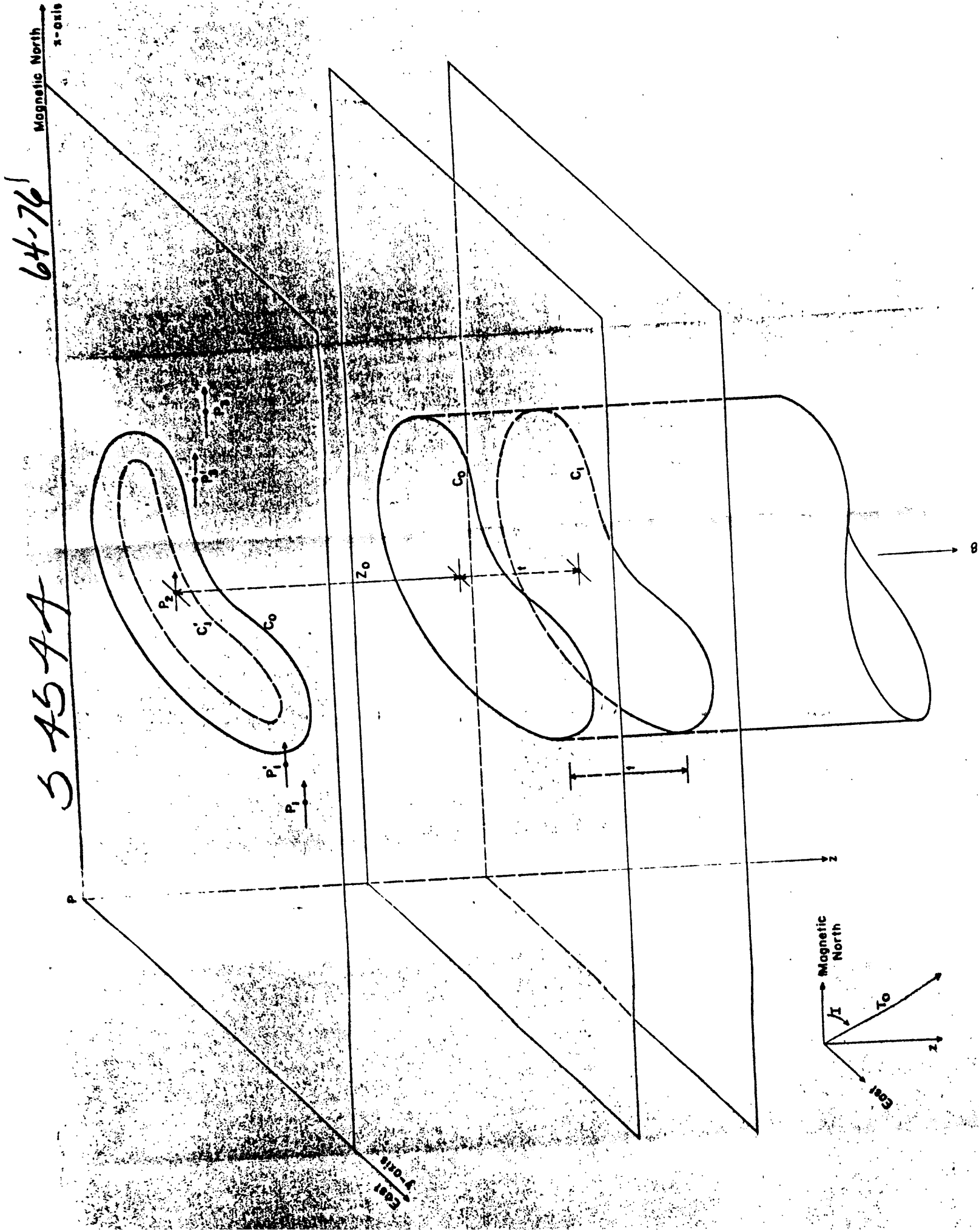
UNIT DEPTH

54544

PLEASE REPLACE IN POCKET
IN BACK OF BOUND

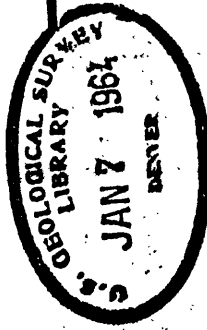
FIG. 2





PLEASE REPLACE IN POCKET
IN BACK OF BOUND VOLUME

Fig. 3. Magnetic effect of cylinder of thickness t derived from effects of two semi-infinite cylinders at depths z_0 and $z_0 + t$. Configuration for lower figure given by primes after reduction to scale by applying factor $z_0/(z_0 + t)$.



64-76

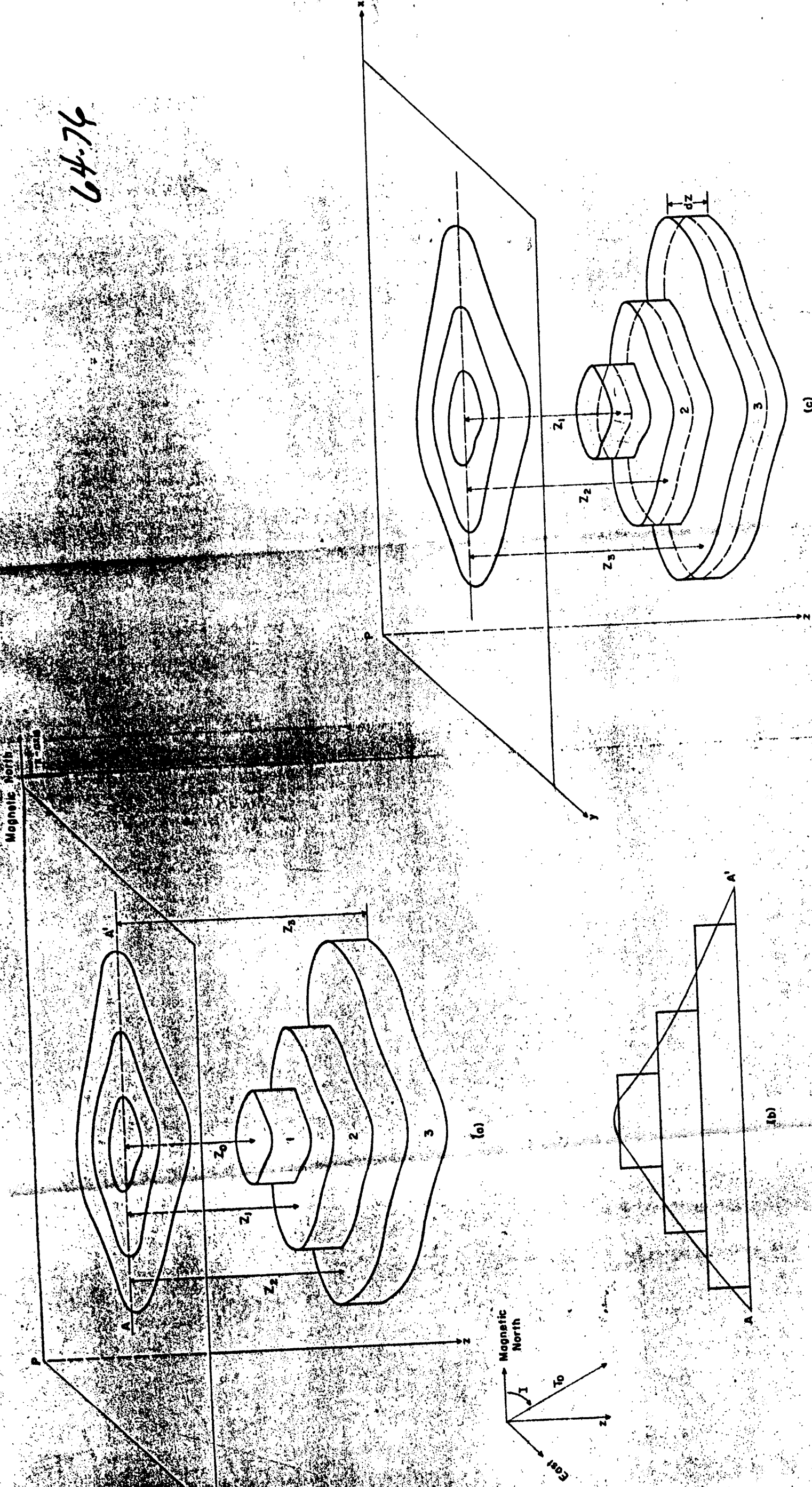
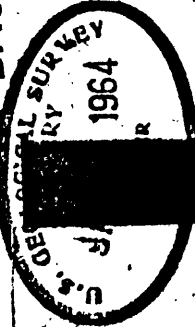


Fig. 4. Three dimensional body approximated with laminae.
 (a) magnetic body; graticule is used at top and bottom of each lamina
 (b) vertical section A-A'
 (c) gravity body; solid angle chart ($I = 90^\circ$) is used at median plane of laminae.

PLEASE REPLACE IN POCKET
 IN BACK OF BOUND VOLUME



54544

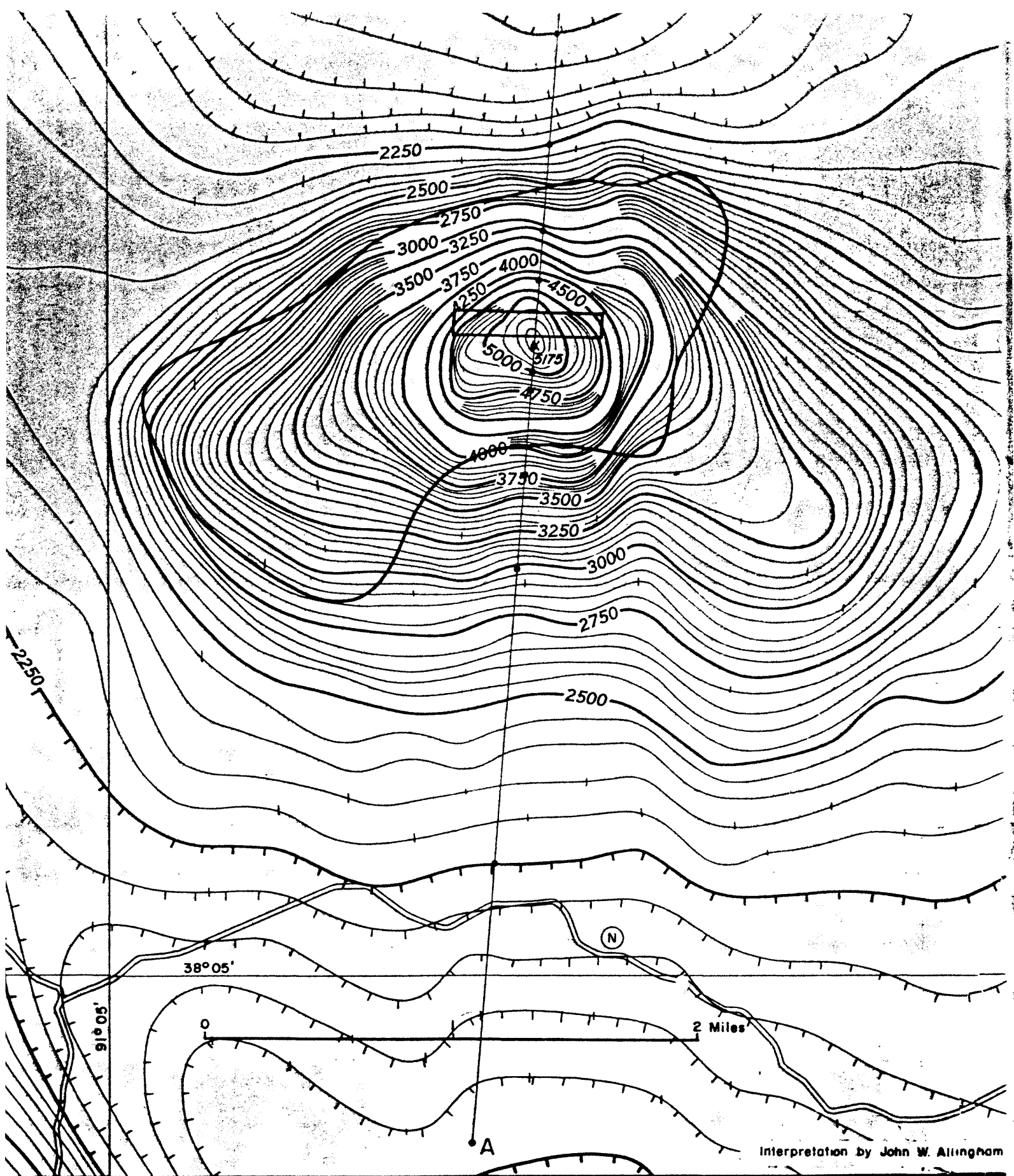
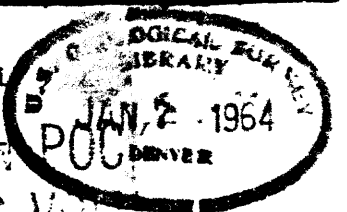
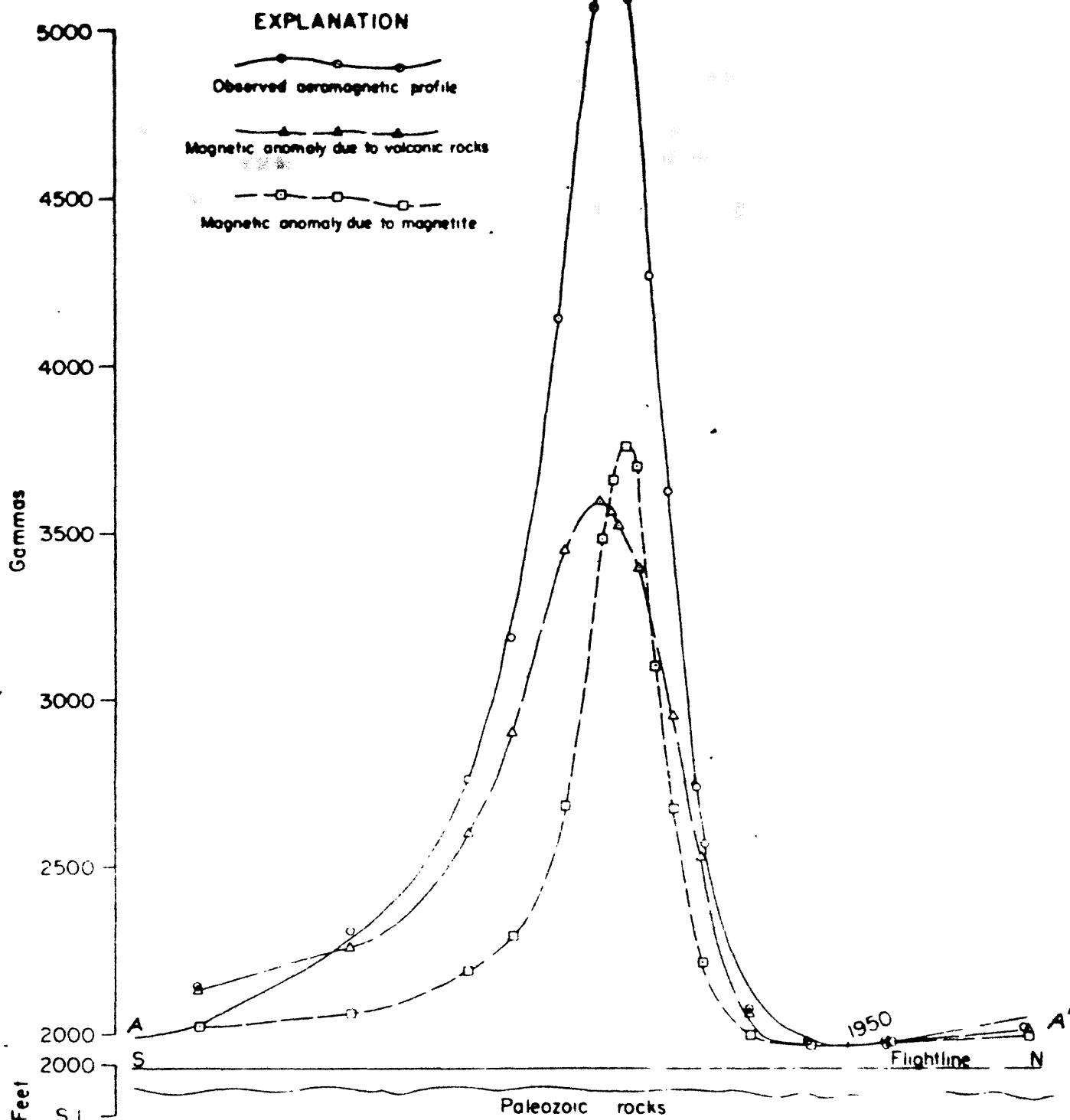


Figure 5. Aeromagnetic map of Pea Ridge anomaly, southeast Missouri. Inferred contact between volcanic rocks and granite host rock shown by heavy irregular line. Rectangle is conjectured outline of ore body.

Interpretation by John W. Allingham



5454A



PLEASE REPLACE IN POCKET
IN BACK OF BOUND VOLUME

5454A

Figure 6. An interpretation of Pea Ridge anomaly

